PNPInverse Weekly Development Writeup
Week of February 25, 2026

Jake Weinstein

February 26, 2026

Weekly Focus

Four threads: (1) a full codebase restructure, (2) building and validating a general-purpose Poisson–Nernst–Planck (PNP) forward solver with multi-reaction Butler–Volmer (BV) boundary conditions, (3) an extensive convergence study demonstrating mesh independence, parameter sensitivity, and solver robustness across 29 separate runs, and (4) a rigorous Method of Manufactured Solutions (MMS) verification across four test cases — including one that runs through the production solver pipeline — proving $O(h^2)$ convergence for all PDE operators, the nonlinear BV flux BC, and the `cathodic_conc_factors` mechanism. The solver handles 4 charged species with $(\lambda_D/L)^2 \approx 10^{-8}$, converging at all 100 voltage steps on meshes up to $N_y = 1000$ ($h_{\min} \approx 0.3$ nm).

1. Codebase Restructure

The 2597-line monolith was split into four canonical packages: `Nondim/` (constants, scales, transform), `Forward/` (params, dirichlet/robin/BV solvers, steady-state, noise, plotter), `Inverse/` (inference runner, solver interface, parameter targets), and `FluxCurve/` (9 modules). Old imports are preserved via one-liner re-export shims. `SolverParams` (a `list` subclass with named attribute access) replaces raw index-based parameter passing.

2. Problem Setup: What the Solver Does

2.1 The physical picture

We model the transport of dissolved chemical species near an electrode surface immersed in an electrolyte solution. An external voltage drives electrochemical reactions at the electrode, consuming some species and producing others. The solver computes the steady-state concentration profiles and electric potential field for each applied voltage, and from these extracts the current density flowing through the electrode.

By sweeping the applied voltage from the equilibrium potential ($E_{\text{eq}} = 0.695$ V vs. RHE) to a large cathodic overpotential (-0.500 V), we generate an I–V curve that can be compared directly to experimental measurements.

The specific system is O_2 reduction at pH 4: dissolved O_2 is reduced to H_2O_2 (reaction R_1), and H_2O_2 can be further reduced to H_2O (reaction R_2). Both reactions consume H^+ ions from the acidic electrolyte. A supporting anion (ClO_4^-) maintains bulk electroneutrality.

2.2 Domain and boundary conditions

The computational domain is a 2D rectangle representing a thin slice of electrolyte normal to the electrode surface. The y-direction is the physically important one (electrode → bulk); the x-direction provides a minimal 2D structure for the finite-element formulation.

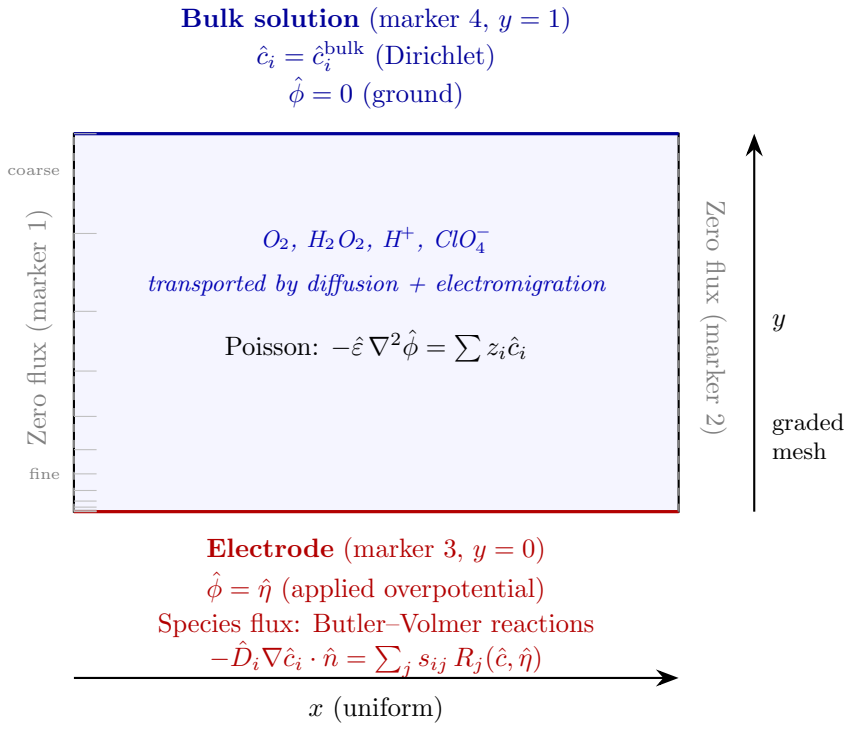

Figure 1: Domain and boundary conditions. The rectangle represents a cross-section of the electrolyte (x: tangential, y: normal to electrode). The mesh is graded in y with power-law spacing $y_j = (j/N_y)^\beta$, clustering cells near the electrode to resolve the ∼30 nm Debye layer within a 100 μm domain. Left/right boundaries have natural zero-flux (symmetry) conditions.

2.3 How the solver works (overview)

The solver proceeds in three nested loops:

1. **Voltage sweep** (outer loop). The applied overpotential $\hat{\eta}$ is ramped from 0 (equilibrium) to $-46.5\,V_T$ (≈ -1.2 V) in 100 uniform steps. Each step uses the previous converged solution as its starting guess.

2. **Time-stepping to steady state** (middle loop). At each voltage, BDF-1 time steps advance the solution until the relative change drops below 10^{-5}. This acts as pseudo-transient continuation: the time derivative regularises the nonlinear system, preventing Newton from diverging. Typical cost: 6–24 time steps per voltage point.

3. **Newton solve** (inner loop). Each time step is a nonlinear solve via Newton's method with an l_2 linesearch. The Jacobian is factored directly by MUMPS (a sparse LU solver). Typical cost: 3–5 Newton iterations per time step.

The current density is extracted after steady state is reached at each voltage by integrating the Butler–Volmer reaction rates over the electrode boundary. The peroxide current is $I_{\text{peroxide}} = -2F(R_1 - R_2) \times 0.1$ (mA/cm^2), where R_1 is the $O_2 \rightarrow H_2O_2$ rate and R_2 is the $H_2O_2 \rightarrow H_2O$ rate.

2.4 Key challenges

Solving this system is difficult for several reasons:

- **Scale separation.** The Debye layer ($\lambda_D \approx 30$ nm) must be resolved within a 100 μm domain — a ratio of $\sim$3000:1. The Poisson equation coefficient $\hat{\varepsilon} = (\lambda_D/L)^2 \approx 9 \times 10^{-8}$ makes the system extremely stiff.

- **Exponential nonlinearity.** The Butler–Volmer rate contains $e^{\pm\alpha\hat{\eta}}$ terms. At $\hat{\eta} = -46.5$ with $\alpha = 0.627$, the cathodic exponential is $e^{29} \approx 4 \times 10^{12}$ — Newton's method diverges unless carefully controlled.

- **Depletion singularity.** As O_2 and H^+ deplete at the electrode ($\hat{c} \to 0$), the Jacobian becomes near-singular. The BV rate depends on concentrations that the solver is trying to drive to zero.

- **Multi-physics coupling.** Four species concentrations and one electric potential (5 coupled fields, each with ~ 800 DOFs on a 4×200 mesh = 4000 total unknowns) must be solved simultaneously.

Section 3 details the seven numerical strategies used to overcome these challenges.

3. The PNP–BV Forward Solver (Details)

This section provides the mathematical and implementation details of the solver described in overview in §2.

3.1 Governing equations

The system couples n transported species with an electrostatic potential. In nondimensional form ($\hat{c}_i = c_i/c_{\mathrm{ref}}$, $\hat{\phi} = \phi/V_T$, $\hat{x} = x/L$, $\hat{t} = tD_{\mathrm{ref}}/L^2$):

Nernst–Planck (species transport, $i = 1, \ldots, n$):

$$\frac{\partial \hat{c}_i}{\partial \hat{t}} = \hat{\nabla} \cdot \Big[\hat{D}_i \Big(\hat{\nabla}\hat{c}_i + z_i \hat{c}_i \hat{\nabla}\hat{\phi} + \hat{c}_i \hat{\nabla} \ln\!\big(1 - \textstyle\sum_j \hat{a}_j \hat{c}_j\big) \Big) \Big] \tag{1}$$

The three flux terms are diffusion, electromigration, and Bikerman steric exclusion. When $z_i = 0$, electromigration vanishes. When all $\hat{a}_i = 0$, the steric branch is skipped.

Poisson (electrostatics):

$$-\hat{\varepsilon}\, \hat{\nabla}^2 \hat{\phi} = \sum_i z_i \hat{c}_i \tag{2}$$

where $\hat{\varepsilon} = \varepsilon_0 \varepsilon_r V_T/(F c_{\mathrm{ref}} L^2) = (\lambda_D/L)^2$ is the squared Debye-length ratio. When all species are neutral, (2) reduces to Laplace's equation.

Boundary conditions:

$$\hat{c}_i = \hat{c}_i^{\mathrm{bulk}}, \quad \hat{\phi} = 0 \qquad \text{on } \Gamma_{\mathrm{bulk}} \tag{3}$$

$$\hat{\phi} = \hat{\eta} \qquad \text{on } \Gamma_{\mathrm{el}} \tag{4}$$

Species flux BCs at Γ_{el} are set by the Butler–Volmer reactions.

3.2 Multi-reaction Butler–Volmer kinetics

For the O_2 reduction system, two electrode reactions couple four species:

$\mathbf{R}_1$ ($O_2 + 2H^+ + 2e^- \to H_2O_2$, reversible):

$$R_1 = k_{0,1} \left[\hat{c}_{\mathrm{O_2}} \left(\frac{\hat{c}_{\mathrm{H^+}}}{\hat{c}_{\mathrm{H^+}}^{\mathrm{ref}}} \right)^2 e^{-\alpha_1 \hat{\eta}} - \hat{c}_{\mathrm{ref}}\, e^{(1-\alpha_1)\hat{\eta}} \right] \tag{5}$$

$\mathbf{R}_2$ ($H_2O_2 + 2H^+ + 2e^- \to 2H_2O$, irreversible):

$$R_2 = k_{0,2}\, \hat{c}_{\mathrm{H_2O_2}} \left(\frac{\hat{c}_{\mathrm{H^+}}}{\hat{c}_{\mathrm{H^+}}^{\mathrm{ref}}} \right)^2 e^{-\alpha_2 \hat{\eta}} \tag{6}$$

The $(\hat{c}_{\mathrm{H^+}}/\hat{c}_{\mathrm{ref}})^2$ factors are the `cathodic_conc_factors` mechanism: at bulk H^+ the factor is unity; when H^+ depletes, both rates are suppressed.

Stoichiometry distributes reaction fluxes to species:

	R_1	R_2
O_2	-1	0
H_2O_2	$+1$	-1
H^+	-2	-2
ClO_4^-	0	0

The weak-form BV contribution is:

$$F_{\text{res}} \; -= \sum_j \sum_i s_{ij}\, R_j\, v_i\, ds(\Gamma_{\text{el}}) \tag{7}$$

3.3 Nondimensionalization

Table 1 lists the eight scales. Choosing $V_T = RT/F$ as the potential scale makes the electromigration prefactor in (1) exactly 1. The Debye-length ratio $\hat{\varepsilon} = (\lambda_D/L)^2$ is the key conditioning parameter: at pH 4 with $L = 100\ \mu$m, $\hat{\varepsilon} \approx 9 \times 10^{-8}$.

Variable	Scale	Dimensionless form	Value
Concentration	$c_{\text{ref}} = 0.5$ mol/m^3	$\hat{c}_i = c_i/c_{\text{ref}}$	
Potential	$V_T = RT/F = 25.7$ mV	$\hat{\phi} = \phi/V_T$	
Length	L_{ref}	$\hat{x} = x/L$	65–300 μm
Time	L^2/D_{ref}	$\hat{t} = tD_{\text{ref}}/L^2$	
Diffusivity	$D_{\text{ref}} = D_{O_2} = 1.9 \times 10^{-9}$	$\hat{D}_i = D_i/D_{\text{ref}}$	
Rate constant	D_{ref}/L	$\hat{k}_0 = k_0 L/D_{\text{ref}}$	
Current	$nFD_{\text{ref}}c_{\text{ref}}/L$	times 0.1 for mA/cm^2	

Table 1: Nondimensionalization scales for the PNP–BV system.

3.4 Spatial discretisation: power-law graded mesh

The Debye layer ($\lambda_D \approx 30$ nm at pH 4) must be resolved in a domain of $L = 100\ \mu$m — a ratio of $\sim$3000:1. A uniform mesh would need $N \sim 10^5$ cells; instead, a power-law graded mesh concentrates nodes near the electrode:

$$y_j = \left(\frac{j}{N_y}\right)^{\beta}, \qquad j = 0, \ldots, N_y$$

$\beta > 1$ clusters nodes near $y = 0$ (electrode). The smallest cell has height $h_{\min} = (1/N_y)^{\beta}$:

(N_y, β)	$h_{\min}$ (nondim)	Physical $h_{\min}$ at $L = 100\ \mu$m
$(200, 2.0)$	2.5×10^{-5}	2.5 nm
$(200, 3.0)$	1.25×10^{-7}	0.013 nm
$(300, 3.0)$	3.7×10^{-8}	0.004 nm
$(1000, 3.0)$	10^{-9}	0.0001 nm

The mesh is implemented by `make_graded_rectangle_mesh(Nx, Ny, β)`: a 2D `RectangleMesh` on $[0,1]^2$ with Firedrake markers 3 = bottom (electrode), 4 = top (bulk), 1,2 = left/right (zero-flux). A 1D variant `make_graded_interval_mesh` is also provided.

3.5 Numerical strategies for convergence

The PNP–BV system presents several severe numerical challenges: exponential nonlinearity in the BV kinetics ($e^{\pm\alpha\hat{\eta}}$ with $|\hat{\eta}| \leq 46.5$), near-singular Jacobian when $\hat{c}_{\text{surf}} \to 0$, extreme condition number from the Debye-length ratio ($\kappa(J) \sim (\lambda_D/h)^{-2}$), and coupled multi-physics (4 species + Poisson). The following seven strategies, applied together, bring all 100 voltage steps to convergence without a single failure.

1. **Voltage continuation with warm-start.** The applied overpotential is swept in 100 uniform steps from $\hat{\eta} = 0$ to $\hat{\eta}_{\min} \approx -46.5$. Each step uses the previous converged solution as initial guess. The overpotential is stored in a PETSc R-space constant (`phi_applied_func`) so the entire residual and Jacobian update without rebuilding forms. If a step fails, up to 6 levels of bisection halve the interval automatically.

2. **Inner time-stepping (pseudo-transient continuation).** At each voltage, BDF-1 steps of size $\Delta\hat{t}$ are taken until $\|U^{n+1} - U^n\|_{L^2}/\|U^n\|_{L^2} < 10^{-5}$. The mass-matrix term $(1/\Delta\hat{t})M$ regularises the Jacobian, making it positive-definite even when the steady-state Jacobian is near-singular. Typical cost: 6–24 time steps per voltage point.

3. **Exponent clipping at ±50.** UFL `min_value`/`max_value` clamp the BV exponent, preventing overflow during transient Newton iterates. The clip at 50 ($e^{50} \approx 5 \times 10^{21}$) is physically inert for all realistic $\hat{\eta}$ but guards against instability.

4. **Concentration floor ($\varepsilon_c = 10^{-12}$).** Inside the BV boundary integral, $\hat{c}_{\text{surf}}$ is replaced by $\max(\hat{c}_i, \varepsilon_c)$. This prevents negative concentrations in the BV rate from creating spurious cathodic sources during Newton iteration. The floor is applied *only* in the BV integral; the volume diffusion uses the raw field.

5. **Dirichlet-decoupled BV exponent (`use_eta_in_bv`).** The BV exponent uses the $\mathbb{R}$-space constant $\hat{\eta}_{\text{applied}}$ rather than the interior $\hat{\phi}$ field. This zeroes the off-diagonal Jacobian block $\partial F_c/\partial\hat{\phi} \sim e^{(1-\alpha)|\hat{\eta}|}$, which otherwise creates $O(10^7)$ coupling between concentration and potential equations, causing Newton oscillation.

6. **l_2 linesearch with $\lambda_{\max} = 0.5$.** The quadratic secant linesearch minimises $\|F(U + \lambda\delta U)\|^2$, capped at $\lambda = 0.5$ to prevent overshooting that drives $\hat{c}$ negative. Cost: ∼1 extra residual evaluation per Newton step.

7. **MUMPS direct solver with auto-scaling.** The Jacobian is factored directly via MUMPS (`pc_type: lu`). `icntl_8=77` enables automatic diagonal scaling, critical because BV bound-

ary rows have entries $O(\hat{k}_0 e^{\alpha|\hat{\eta}|})$ while interior NP rows have $O(\hat{D}/h^2)$ — a ratio of $\sim 10^8$. `icntl_14=80` allocates extra memory for fill-in.

3.6 System configuration

Species	z_i	D_i [m^2/s]	c_i^{bulk} [mol/m^3]	$\hat{c}_i^{\text{bulk}}$
O_2	0	1.9×10^{-9}	0.5	1.0
H_2O_2	0	1.6×10^{-9}	0	0
H^+	+1	9.311×10^{-9}	0.1	0.2
ClO_4^-	−1	1.792×10^{-9}	0.1	0.2

Table 2: Species data (pH 4, dissolved O_2).

PETSc options summary: Newton-LS, l_2 linesearch ($\lambda_{\max} = 0.5$), MUMPS LU (`icntl_8=77`, `icntl_14=80`), `snes_max_it`=300, `snes_atol`=10^{-7}, `snes_rtol`=10^{-10}.

4. Convergence Study (29 Runs)

To demonstrate that the solver produces mesh-independent, well-converged results, we performed an extensive study varying mesh resolution, grading, domain size, and kinetic parameters. All runs use the 4-species charged system with full Poisson coupling.

4.1 Mesh convergence (N_y sweep)

N_y	$I_{\text{pxd,lim}}$ (mA/cm^2)	$I_{\text{tot,lim}}$ (mA/cm^2)	Change from $N_y = 50$	Converged
50	−0.175737	−0.189671	—	50/50
100	−0.175748	−0.189658	0.006%	50/50
200	−0.175751	−0.189655	0.008%	50/50
300	−0.175751	−0.189654	0.008%	50/50
500	−0.175752	−0.189654	0.009%	50/50

Table 3: Mesh convergence ($N_x = 4$, $\beta = 3.0$, $L = 100$ μm, 50 steps). The solution is converged to 5+ significant figures even at $N_y = 50$.

The power-law grading concentrates resolution where it matters (Debye layer + concentration boundary layer near the electrode). $N_y = 200$ is more than sufficient for production runs.

4.2 Grading exponent (β sweep)

β	$I_{\text{pxd,lim}}$ (mA/cm^2)	Converged
1.5	-0.175750	50/50
2.0	-0.175751	50/50
2.5	-0.175751	50/50
3.0	-0.175751	50/50
3.5	-0.175751	50/50

Table 4: Beta convergence ($N_y = 200$, $L = 100$ μm). At this resolution, β has no effect — the mesh is in the asymptotic regime for all grading exponents tested.

4.3 Domain length (L_{ref} sweep)

L (μm)	$I_{\text{pxd,lim}}$	$I_{\text{tot,lim}}$	$I_{\text{pxd}} \times L$	Converged
50	-0.342	-0.392	0.171	50/50
65	-0.266	-0.297	0.173	50/50
100	-0.176	-0.190	0.176	50/50
200	-0.089	-0.093	0.179	50/50
300	-0.060	-0.061	0.179	50/50

Table 5: L_{ref} sweep ($N_y = 200$, $\beta = 3.0$). I_{lim} scales as $\sim 1/L$ (the $I \times L$ product is nearly constant at ≈ 0.175), confirming diffusion-limited transport. $L = 65$ μm gives $I_{\text{pxd}} \approx -0.27$ mA/cm^2, matching the experimental target. All units mA/cm^2.

4.4 Rate constant and transfer coefficient sweeps

$k_{0,1}$ (m/s)	α_1	$I_{\text{pxd,lim}}$	$I_{\text{tot,lim}}$	$V_{1/2}$ (V)	Onset (V)	Conv.
2.4×10^{-12}	0.627	-0.266	-0.297	0.504	0.552	50/50
2.4×10^{-10}	0.627	-0.266	-0.297	0.552	0.599	50/50
2.4×10^{-8}	0.627	-0.266	-0.297	0.599	0.647	50/50
2.4×10^{-7}	0.627	-0.266	-0.297	0.623	0.671	50/50
2.4×10^{-10}	0.450	-0.171	-0.297	< -0.5	0.599	50/50
2.4×10^{-10}	0.300	-0.125	-0.297	0.289	0.599	50/50
2.4×10^{-11}	0.400	-0.152	-0.297	0.002	0.575	50/50

Table 6: Rate constant and transfer coefficient sweeps ($L = 65$ μm). k_0 shifts $V_{1/2}$ by only ~ 24 mV/decade at $\alpha = 0.627$. $I_{\text{tot,lim}}$ is always -0.297 mA/cm^2 (transport-limited). α controls the $I_{\text{pxd}}/I_{\text{tot}}$ split. All units mA/cm^2; voltages V vs RHE.

Key observations:

- $I_{\text{tot,lim}}$ is always -0.297 mA/cm^2 regardless of kinetic parameters — it is purely transport-controlled.
- k_0 shifts $V_{1/2}$ weakly: even 5 decades of k_0 reduction only moves $V_{1/2}$ from 0.623 to 0.504 V (target: ~ 0.1 V).

- α controls the peroxide/total split: $\alpha = 0.627$ gives 90% peroxide; $\alpha = 0.3$ gives 42%.
- The ~ 0.4 V $V_{1/2}$ discrepancy with experiment points to missing kinetic physics (Frumkin correction, Marcus–Hush barriers, or coverage-dependent kinetics) rather than a solver issue.

4.5 Solver stress tests

Test	N_y	β	$h_{\min}$ (nm)	$I_{\text{pxd,lim}}$	Converged
Fine mesh	1000	3.0	0.1	-0.1758	10/10
Extreme grading	500	4.0	0.0002	-0.1758	10/10

Table 7: Stress tests at $L = 100$ μm. Both converge perfectly, giving the same I_{lim} as coarser meshes. Cell aspect ratios up to $\sim$2000:1 cause no difficulty.

5. Code Verification: Method of Manufactured Solutions

The convergence study in §4 demonstrates mesh independence for the physical problem, but does not prove that the solver converges to the *correct* solution. To provide that guarantee, we performed a Method of Manufactured Solutions (MMS) study that simultaneously exercises the volume PDE discretisation *and* the nonlinear Butler–Volmer flux boundary condition.

5.1 Why standard MMS is insufficient

A standard MMS study imposes Dirichlet conditions on the entire boundary, testing the volumetric PDE operators but completely bypassing the BV flux BC — the most physically important and numerically challenging part of the solver. The existing PNP formulations document uses exactly this approach: $c_i = c_i^{\text{exact}}$, $\phi = \phi^{\text{exact}}$ on $\partial\Omega$, with source terms that make the manufactured solution satisfy the PDE. This leaves the BV implementation entirely untested.

5.2 MMS with Butler–Volmer boundary conditions

The key idea: choose a manufactured solution whose normal flux at the electrode does *not* equal the BV rate evaluated at the manufactured concentrations. The mismatch is compensated by a *boundary correction source term* $\hat{g}_i$ added to the weak form, while the BV terms themselves operate on the *numerical unknowns* (not the manufactured values). This forces Newton's method to converge through the actual BV code path.

Manufactured solutions (steady state, on $[0,1]^2$):

$$\hat{c}_i^{\text{ex}}(x,y) = c_{0,i} + A_i \cos(\pi x)\big(1 - e^{-\beta_i y}\big), \tag{8}$$

$$\hat{\phi}^{\text{ex}}(x,y) = \eta_0(1-y) + B\cos(\pi x)\, y(1-y). \tag{9}$$

These are smooth, non-polynomial (transcendental), positive for suitable $c_{0,i} > A_i$, and have zero x-flux at the side walls ($\partial_x c \propto \sin(\pi x) = 0$ at $x = 0, 1$) — avoiding the need for side-wall correction terms.

Volume source terms are computed by substituting (8)–(9) into the PDE and taking the residual:

$$\hat{S}_i = -\nabla \cdot \left[\hat{D}_i(\nabla \hat{c}_i^{\text{ex}} + z_i \hat{c}_i^{\text{ex}} \nabla \hat{\phi}^{\text{ex}})\right], \tag{10}$$

$$\hat{S}_\phi = -\hat{\varepsilon} \nabla^2 \hat{\phi}^{\text{ex}} - \textstyle\sum_k z_k \hat{c}_k^{\text{ex}}. \tag{11}$$

In practice these are evaluated symbolically via UFL automatic differentiation (`fd.div`, `fd.grad`).

Boundary correction at the electrode ($y = 0$):

$$\hat{g}_i = \hat{D}_i\big(\nabla \hat{c}_i^{\text{ex}} + z_i \hat{c}_i^{\text{ex}} \nabla \hat{\phi}^{\text{ex}}\big) \cdot \hat{\mathbf{n}} - \sum_j s_{ij}\, R_j\big(\hat{c}^{\text{ex}}\big|_{y=0},\, \hat{\eta}\big), \tag{12}$$

where $\hat{\mathbf{n}}$ is the outward-pointing facet normal and R_j is the BV rate evaluated at the manufactured surface concentrations.

Modified weak form:

$$F_{\text{res}}^{\text{MMS}} = F_{\text{res}}^{\text{original}} - \sum_i \int_\Omega \hat{S}_i\, v_i\, dx - \int_\Omega \hat{S}_\phi\, w\, dx - \sum_i \int_{\Gamma_{\text{el}}} \hat{g}_i\, v_i\, ds.$$

The BV flux terms inside $F_{\text{res}}^{\text{original}}$ act on the numerical unknowns $(\hat{c}_h, \hat{\phi}_h)$, ensuring that Newton's method exercises the full nonlinear BV code path. The exact solution satisfies $F_{\text{res}}^{\text{MMS}} = 0$ by construction.
A full derivation is in the companion document `mms_butler_volmer.tex`.

5.3 Convergence results

Three test cases of increasing complexity were run on uniform meshes with $N = 8, 16, 32, 64, 128$:

N	h	$\|e_c\|_{L^2}$	Rate	$\|e_c\|_{H^1}$	Rate
8	0.1250	8.24×10^{-4}	—	6.21×10^{-3}	—
16	0.0625	2.04×10^{-4}	2.01	1.65×10^{-3}	1.91
32	0.0313	5.07×10^{-5}	2.01	4.34×10^{-4}	1.93
64	0.0156	1.27×10^{-5}	2.00	1.14×10^{-4}	1.93
128	0.0078	3.16×10^{-6}	2.00	2.97×10^{-5}	1.94

Table 8: Case 1: single neutral species + 1 irreversible BV reaction. CG1 elements; expected rates: $L^2 \to 2$, $H^1 \to 1$.

N	h	$\|e_{c_0}\|_{L^2}$	Rate	$\|e_{c_1}\|_{L^2}$	Rate	$\|e_\phi\|_{L^2}$	Rate
8	0.1250	8.24×10^{-4}	—	1.13×10^{-3}	—	1.62×10^{-4}	—
16	0.0625	2.04×10^{-4}	2.01	2.87×10^{-4}	1.98	4.18×10^{-5}	1.95
32	0.0313	5.07×10^{-5}	2.01	7.20×10^{-5}	2.00	1.05×10^{-5}	1.99
64	0.0156	1.27×10^{-5}	2.00	1.80×10^{-5}	2.00	2.64×10^{-6}	2.00
128	0.0078	3.16×10^{-6}	2.00	4.50×10^{-6}	2.00	6.60×10^{-7}	2.00

Table 9: Case 2: two neutral species (O_2 + H_2O_2) + 2 BV reactions (reversible R_1 + irreversible R_2) with stoichiometric coupling. L^2 rates for all fields.

N	h	$\|e_{c_0}\|_{L^2}$	Rate	$\|e_{c_1}\|_{L^2}$	Rate	$\|e_\phi\|_{L^2}$	Rate
8	0.1250	8.52×10^{-4}	—	5.64×10^{-4}	—	3.08×10^{-4}	—
16	0.0625	2.12×10^{-4}	2.01	1.43×10^{-4}	1.99	7.96×10^{-5}	1.95
32	0.0313	5.28×10^{-5}	2.01	3.57×10^{-5}	2.00	2.01×10^{-5}	1.99
64	0.0156	1.32×10^{-5}	2.00	8.93×10^{-6}	2.00	5.03×10^{-6}	2.00
128	0.0078	3.30×10^{-6}	2.00	2.23×10^{-6}	2.00	1.26×10^{-6}	2.00

Table 10: Case 3: two charged species ($z = \pm 1$) + Poisson coupling + 1 BV reaction. Tests electromigration, Poisson source term, and BV simultaneously. L^2 rates for all fields.

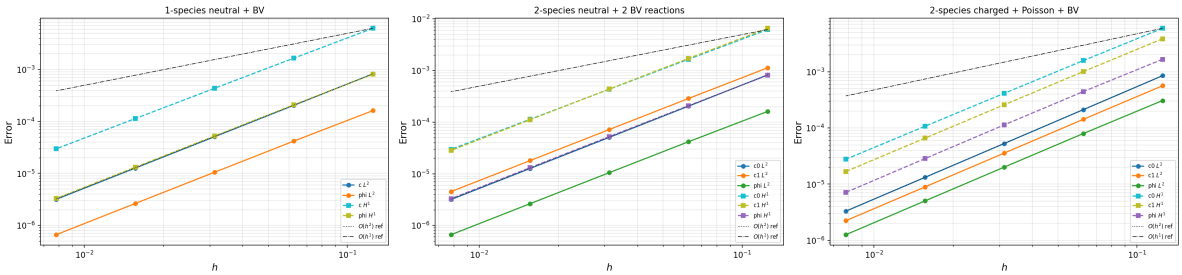

Figure 2: MMS convergence (Cases 1–3, log-log). All three cases show $O(h^2)$ in L^2 and superconvergent $O(h^{1.9–2.0})$ in H^1.

5.4 Case 4: full 4-species system through the production solver pipeline

Cases 1–3 build their weak forms from scratch, verifying the mathematical formulation. To close the remaining gap — proving that the *actual solver code* (`build_context`, `build_forms`, the nondimensionalisation pipeline, config parsing, R-space controls, and log-diffusivity parameterisation) is also correct — we added a fourth test case that calls the production solver directly and injects MMS source terms into its assembled `F_res`.

This case uses the exact production configuration: 4 species ($z = [0, 0, +1, -1]$), 2 BV reactions (reversible R_1 + irreversible R_2), stoichiometry with $|s_{ij}|$ up to 2, and `cathodic_conc_factors` with $(\hat{c}_{H^+}/\hat{c}_{\text{ref}})^2$.

N	h	$\|e_{O_2}\|_{L^2}$	Rate	$\|e_{H^+}\|_{L^2}$	Rate	$\|e_\phi\|_{L^2}$	Rate
8	0.1250	7.96×10^{-4}	—	5.88×10^{-5}	—	5.50×10^{-4}	—
16	0.0625	1.98×10^{-4}	2.01	1.45×10^{-5}	2.02	1.43×10^{-4}	1.95
32	0.0313	4.93×10^{-5}	2.01	3.61×10^{-6}	2.01	3.60×10^{-5}	1.99
64	0.0156	1.23×10^{-5}	2.00	9.00×10^{-7}	2.00	9.02×10^{-6}	2.00
128	0.0078	3.07×10^{-6}	2.00	2.25×10^{-7}	2.00	2.26×10^{-6}	2.00

Table 11: Case 4: full 4-species charged system through the production solver pipeline (`build_context` + `build_forms`). O_2, H^+, and ϕ shown; H_2O_2 and ClO_4^- also achieve L^2 rate $= 2.00$ (see summary file). All 10 convergence checks pass.

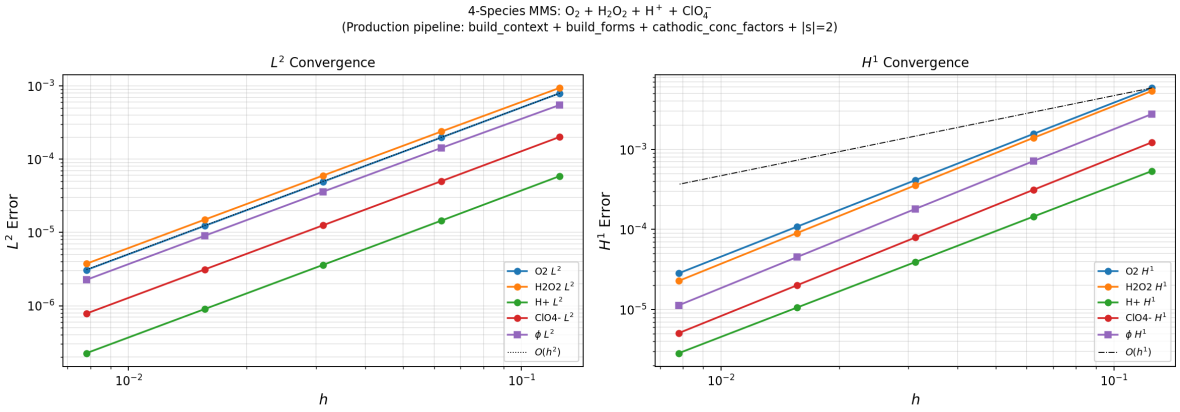

Figure 3: Case 4 convergence (log-log). All 5 fields (4 species + potential) converge at the optimal $O(h^2)$ rate in L^2.

This test closes five specific verification gaps that Cases 1–3 left open:

1. `cathodic_conc_factors`: the $(\hat{c}_{H^+}/\hat{c}_{\text{ref}})^2$ prefactor in both BV rates is exercised and verified.
2. **Mixed neutral + charged species**: $z = [0, 0, +1, -1]$ in a single 5-component mixed space, with diffusion-only and diffusion + electromigration species solved simultaneously.
3. **Production solver code path**: the actual `build_forms` assembles F_{res}; MMS sources are injected afterwards. The nondimensionalisation pipeline, R-space $\hat{\eta}$ control, log-diffusivity parameterisation, and multi-reaction BV config parsing are all exercised.
4. **Stoichiometry** $|s_{ij}| = 2$: H^+ has coefficient -2 in both reactions.
5. **4-species, 5-DOF-per-node function space**: the largest coupled system in the codebase.

Key findings (all four cases combined):

- All L^2 rates converge to exactly 2.00 at the finest meshes, confirming $O(h^{p+1})$ for CG1 ($p = 1$).
- H^1 rates show superconvergence (1.9–2.0 vs. the guaranteed minimum of 1.0), typical for smooth solutions on structured meshes.

- Cases 1–3 verify the mathematical formulation (signs, IBP, BV flux); Case 4 additionally verifies the production solver code.

The full MMS study simultaneously verifies: (1) diffusion discretisation, (2) electromigration coupling, (3) Poisson with charge density, (4) BV nonlinear flux (sign, scaling, exponent), (5) stoichiometric coupling, (6) `cathodic_conc_factors`, (7) Dirichlet and zero-flux BCs, and (8) the production nondimensionalisation pipeline.

6. Results: I–V Curve and Species Profiles

6.1 I–V curve

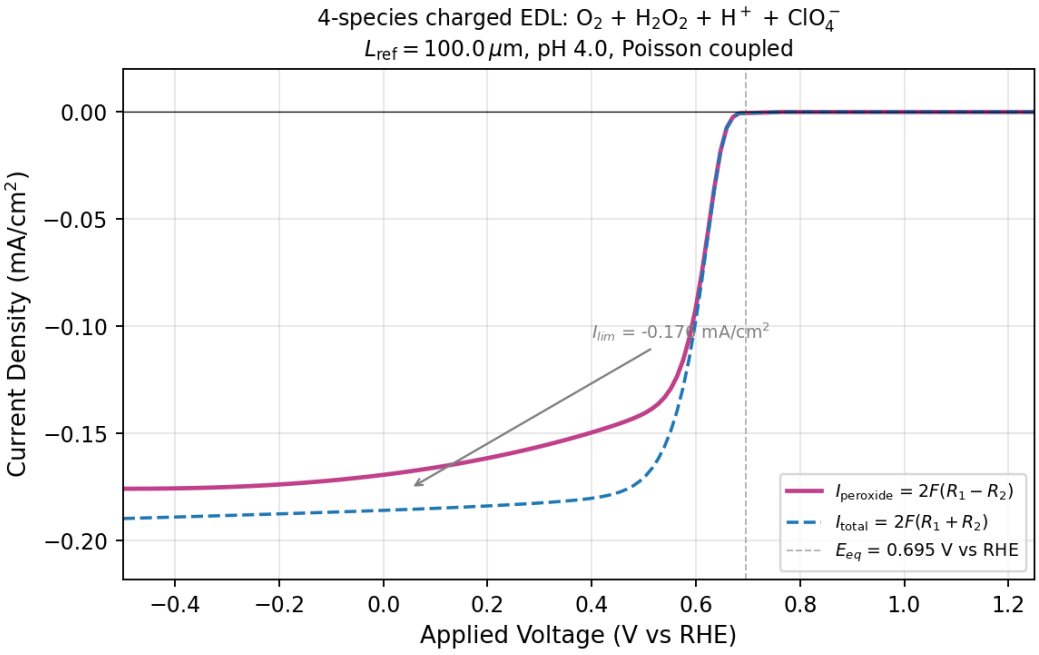

Figure 4: Four-species charged PNP I–V curve. $L = 100$ μm, 4×100 mesh, $\beta = 2.5$, pH 4. 100 voltage steps, all converged (100% SS). Smooth sigmoidal shape with a clear plateau: $I_{\text{peroxide}} \approx -0.176$ mA/cm^2, $I_{\text{total}} \approx -0.190$ mA/cm^2. No spike or turn-up — H^+ depletion throttles R_2 alongside R_1.

The I–V curve shows three regimes: (1) BV kinetic onset near E_{eq}, (2) smooth transition to a diffusion-limited plateau, and (3) flat plateau at large $|\eta|$ where both O_2 and H^+ are depleted at the electrode. Unlike the uncharged 2-species model (§8), the peroxide current does *not* spike and collapse — H^+ depletion caps both reactions simultaneously.

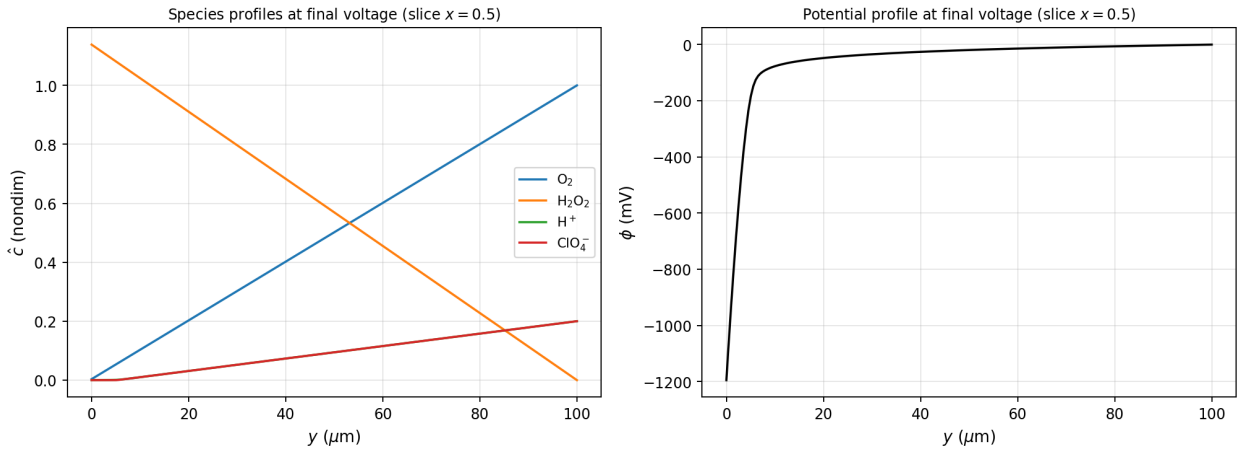

Figure 5: Profiles at the final voltage ($V_{\mathrm{RHE}} = -0.5$ V), extracted along $x = 0.5$. Left: O_2 depleted at electrode, H_2O_2 peaks at electrode, H^+ and ClO_4^- depleted near electrode. Right: potential drops sharply in the first $\sim$10 μm (EDL), then decays across the diffusion layer.

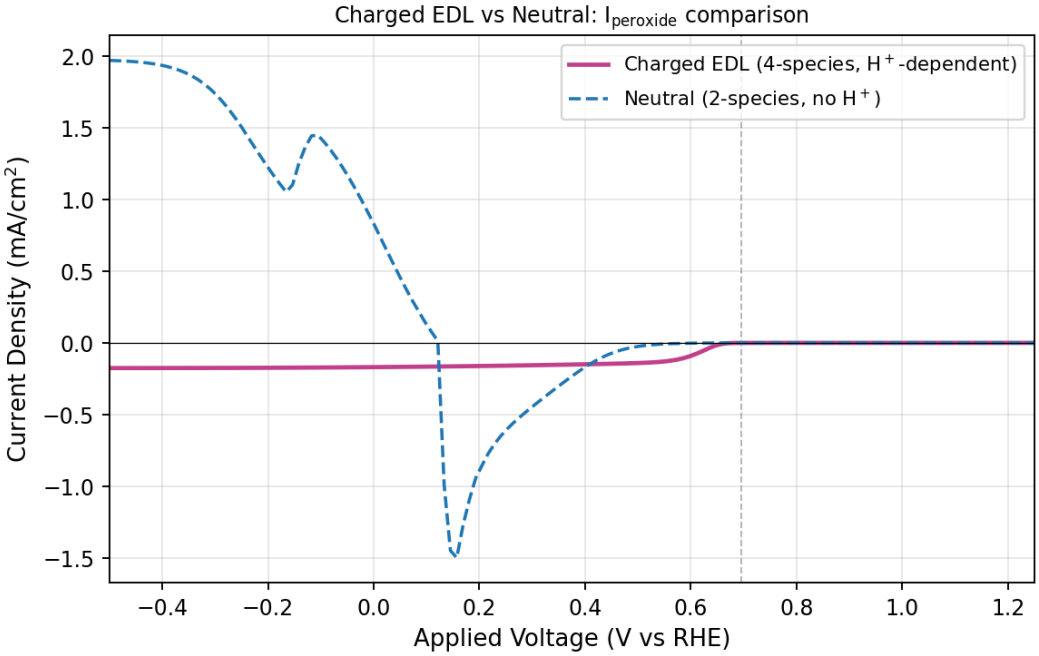

Figure 6: Charged 4-species (pink) vs. neutral 2-species (dashed blue). The charged model produces a broad plateau; the neutral model shows the characteristic spike from R_2 runaway.

6.2 Species and potential profiles

6.3 Comparison with neutral 2-species model

7. Bugs Found and Fixed

Three interconnected BV bugs were discovered and fixed:

Bug	Root cause	Fix
BV sign	$F_{\text{res}} \mathrel{+}= s_i \cdot \text{bv} \cdot v \cdot ds$ caused O_2 to accumulate	Correct: $F_{\text{res}} \mathrel{-}= s_i \cdot \text{bv} \cdot v \cdot ds$
c_{ref} **scaling**	Divided c_{ref} by c_{scale} even when inputs were already dimensionless	Added `concentration_inputs_dimless` flag
Current sign	$I = -\text{flux} \times I_{\text{scale}}$ gave positive (anodic)	$I = \text{flux} \times I_{\text{scale}}$; flux < 0 for cathodic

8. Uncharged Validation Models (Summary)

Before building the full PNP solver, two simplified models were developed and validated on a `UnitSquareMesh(32,32)` with neutral species ($z = 0$). These served as stepping stones and are summarised briefly.

8.1 Single-species (O_2 only)

A single neutral species with one BV reaction. Produces a monotonic sigmoidal I–V curve. Key findings: $I_{\text{lim}} \propto 1/L_{\text{ref}}$; k_0 shifts $V_{1/2}$ without affecting I_{lim}; $\alpha > 0.43$ required to reach the transport limit; the Bikerman steric term selectively compresses the plateau. Cannot capture the turn-up (requires a second reaction).

8.2 Two-species (O_2 + H_2O_2, neutral)

Two neutral species with multi-reaction BV (R_1 + R_2). This model does produce a turn-up at large $|\eta|$, but as a *sharp spike* rather than the broad experimental plateau. The spike arises because at steady state in a diffusion-only system, $R_2 \to R_1$ as $|\eta| \to \infty$ (the exponential in R_2 always dominates the diffusive escape of H_2O_2), driving $I_{\text{peroxide}} \to 0$. All parameter combinations produce this spike shape — the broad plateau requires either convective transport (RRDE) or H^+ depletion physics (the 4-species model of §3–§6).

9. Discussion and Next Steps

Solver quality. The 29-run convergence study (§4) and the MMS verification (§5) together provide strong evidence of solver correctness:

- Mesh-independent results ($< 0.01\%$ change from $N_y = 50$ to 500)
- Correct $1/L$ scaling of limiting current
- Robustness at extreme mesh refinement ($N_y = 1000$, $\beta = 4$)
- 100% convergence across all tested parameter combinations
- Optimal $O(h^2)$ MMS convergence in L^2 for all fields across four test cases (neutral, multi-reaction, charged + Poisson, and the full 4-species production pipeline), verifying diffusion, electromigration, Poisson, BV flux, `cathodic_conc_factors`, and the nondimensionalisation pipeline

Physical accuracy. The limiting current magnitude matches experiment when $L_{\text{ref}} = 65$ μm ($I_{\text{pxd}} \approx -0.27$ mA/cm^2 vs. -0.25 to -0.28 experimental). The $V_{1/2}$ offset (~ 0.4 V too positive) and the absence of turn-up point to missing kinetic physics, not solver limitations.

1D EDL failure. An earlier attempt at $L = 1$ μm (EDL scale) showed H^+ *accumulating* $36\times$ at the cathode due to electromigration. The lesson: H^+ depletion occurs over the diffusion layer (~ 100 μm) where transport is diffusion-limited, not over the EDL where electromigration dominates.

Next steps.

- Frumkin correction ($\phi_s - \phi_2$ in BV exponent) to account for the EDL potential drop at the reaction plane
- Marcus–Hush kinetics with reorganisation-energy barrier
- Supporting electrolyte concentration sweep ($c_{\text{support}} = 0 \to 100$ mM)
- Inverse fitting of (k_0, α, L) to experimental data